Modeling of Litz Wire Winding AC Resistance Based on Improved Segmented Equivalent Circuit

Yueyin Wang, *Student Member, IEEE*, Wu Chen, *Senior Member, IEEE*, and Zhan Shen, *Member, IEEE*

***Abstract*—Litz wire is a promising solution for reducing winding loss in high-frequency magnetics, but modeling its ac resistance remains a challenge. This article proposes the improved segmented circuit method (iSEC) for modeling the ac resistance of concentric and composite litz wires. The method approximates the twisting effect of litz wire by using segmented parallel strands that are cascaded into segmented circuits. The segmented circuit is then simplified to a matrix calculation based on the twisting characteristics, reducing computational consumption while maintaining accuracy. The impedance matrix is calculated using the one-dimensional field and the proposed modified coefficient. Consequently, iSEC can fully analytically calculate the ac resistance of concentric and composite wires. The method is validated in the 2 MHz range using transformer samples with various configurations, and the average error in the studied cases is 11.1%.**

***Index Terms*—AC resistance, litz wire, transformer, winding loss.**

I. Introduction

THE development of power electronics enables the wide-range applications of grid-connected renewable energy sources [1], [2], [3], e.g., photovoltaics, wind turbines, etc. High-frequency transformers play a vital role in those high-power converters [4], [5]. Generally, it is preferred to increase the operating frequency of the transformer to reduce cost and increase power density. However, it also increases in winding losses and temperature, which limits the size and efficiency of transformers [6], [7].

Litz wires are commonly used to mitigate the high-frequency effects of windings. However, the three-dimensional (3-D) stranded structure makes it challenging to calculate losses accurately. The finite-element method (FEM) is a widely used numerical technique for physical field calculations. Despite its fast speed, the usual 2-D FEM method does not account for bundel-level skin and proximity effects, which results in the underestimation of the ac loss of litz wire [8]. Although 3-D litz wire modeling can overcome this issue, its application is time-consuming due to the helical and void-free structure. To address this issue, researchers have developed approaches to speed up it, such as homogenizing the wire [9], [10]. Despite these methods, achieving accurate results still requires cumbersome preprocessing, including geometric modeling and physical field setup, as well as complicated mesh-independent analysis.

Among other numerical methods, partial element equivalent circuit (PEEC) is a promising method that approximates the magnetic field problem with an equivalent circuit and has been further developed [11]. Although PEEC reduces the computation time relative to FEM, it discretizes the structure using cuboids, which is not feasible for large numbers of strands or large systems. Strand element equivalent circuit (SEEC) addresses this problem by considering the strand as a single discrete element [12]. Furthermore, the sparse inductance matrix obtained by separating the near and far field leads to a higher speed [13]. While the evolution of PEEC is promising, numerical discretization of complex structure still burdens the calculation and require tradeoffs between accuracy and speed.

The semi-empirical model offers high accuracy by utilizing a mathematical model based on substantial data points, which results in great computational efficiency for subsequent calculations [14], [15]. With the advancement of artificial intelligence, the method has been further developed, demonstrating good accuracy and numerical stability [16], [17]. However, such methods require extensive training time and data points within the defined configuration parameter range. For transformer configuration beyond the defined range, the applicability of the semiempirical method remains questionable.

The analytical approach is a physically derived, efficient method that has been used for automatic iterative optimization. Researchers have developed accurate analytical methods for high-frequency loss using Dowell model [18]. Modifications proposed in [19] and [20] broaden the method application to Faraday-shield [21] and multistranded circular conductors [22]. However, certain analytical methods assume homogeneous current within all strands by ideal litz constructions [23]. An approximate model for litz-wire winding was proposed in [24], assuming equal net currents of all strands, which is only applicable to composite litz wires where whole homogeneous current can be achieved.

Moreover, most literatures have focused on composite litz wire, to the author's knowledge. The same number of strands may result in different frequency-dependent resistances [25], and the current distribution in concentric wires (c.f. Fig. 1) differs from that of composite wires, making it challenging to apply equal-current-based method directly to the concentric

Manuscript received 26 February 2023; revised 6 June 2023 and 17 August 2023; accepted 25 September 2023. Date of publication 2 October 2023; date of current version 6 December 2023. This work was supported by the National Natural Science Foundation of China under Grant 51922028. Recommended for publication by Associate Editor Y. Siwakoti. *(Corresponding author: Wu Chen.)*

The authors are with the Center for Advanced Power Conversion Technology and Equipment, School of Electrical Engineering, Southeast University, Nanjing 210096, China (e-mail: wangyueyin1@163.com; chenwu@seu.edu.cn; zhs@seu.edu.cn).

Color versions of one or more figures in this article are available at https://doi.org/10.1109/TPEL.2023.3321327.

Digital Object Identifier 10.1109/TPEL.2023.3321327

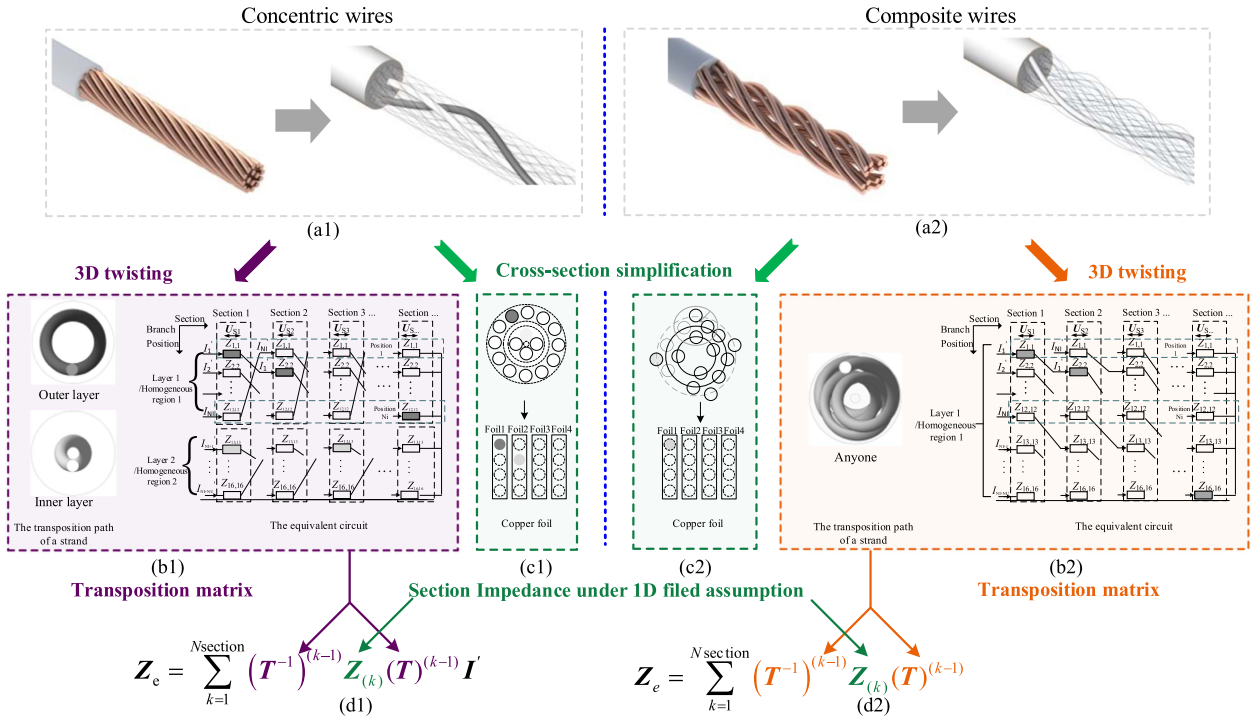

Fig. 1. Geometric configurations, transposition method, and the difference between concentric and composite wires. (a) Structure of two types of litz wires and specific strands highlighted within the wires. (b) Transposition path of the highlighted strands and the corresponding equivalent circuit. (c) Simplified geometry used for calculating section impedance. (d) Calculating formula for the equivalent impedance matrix of the litz wire, where $\boldsymbol{Z}_e$ is the equivalent impedance matrix of the litz wire, $\boldsymbol{T}$ is the transposition matrix, and $\boldsymbol{Z}_{(k)}$ is the section impedance.

wires. As a result, there is a need to develop an improved loss model for litz wire that account for diverse twisting patterns and nonuniform current distributions.

Chen and Xu [26] proposed the segmented equivalent circuit (SEC) method to address nonuniform current distribution in concentric strands by considering the specific twisting pattern. Despite its high accuracy, it relies on FEMs, which can be consuming and challenging to apply to designs requiring iterative optimization. Furthermore, the original SEC only considers concentric wires, which is suitable for a small number of strands. These limitations pose a significant obstacle to the practical application.

This article proposes an improved segmented circuit (iSEC) model to address the above limitations and offers the following four contributions:

1) The proposed method is an ac loss analytical method applicable to both concentric and composite litz wires.
2) The method is derived from the discrete circuit and condensed to an analytical approach based on simplified axial magnetic field. It has a wider range of applicability than the conventional equal-current-based method.
3) Improved accuracy is achieved by using proposed physically based coefficients to modify errors caused by geometric simplifications.
4) Distinguished from the original SEC, iSEC is fully analytical and the application is extended to composite strands—a practical litz construction.

The rest of the article is organized as follows. Section II outlines the simplifications and assumptions made for both structures and analyzes the magnetic field to derive the ac impedance. In addition, the physically based coefficients are proposed to correct errors resulting from geometric simplifications, yielding the section impedance—the basic element of the equivalent circuit described in Section III. The circuit provides ac resistances for concentric and composite wires by cascading the strands, which are further condensed to a matrix calculation. Section IV presents experimental and computational results, along with comparison to other methods. There are two common litz wires, concentric and composite wire, studied in the article. The proposed computational concept can be summarized as follows: the impedance characteristics of litz wires depend on the equivalent circuit connections reflecting the twisting pattern and the section impedance in them. The corresponding chapters and formulas in the article are presented in the form of a computational instruction in Fig. 2. Finally, Section V concludes this article.

II. Procedure 1: Section Impedance Calculation

The original SEC calculation procedure is outlined in subsection A. Subsection B covers the geometric transformation of the litz wire, including its assumptions and limitations. Further, subsections C, D, and E derive the section impedance.

A. Original Segmented Equivalent Circuit Method

SEC was proposed by Chen and Xu [26] in a Chinese paper. The core idea is to approximate the concentric stranded wire with parallel-wound wires as shown in Fig. 3.

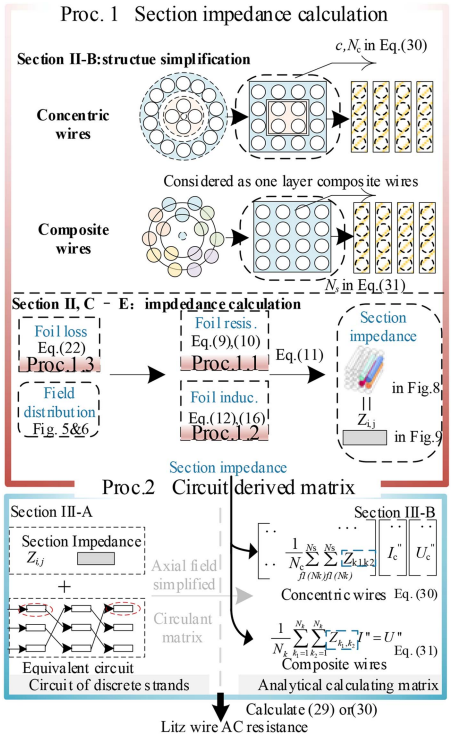

Fig. 2. Computational instruction of the method and the connection of each section. The calculation flow can be summarized in the following steps: procedure 1: The circular strands is converted into foils. Then, the ac impedance of the foils are calculated using a 1-D field model and then transformed into the section impedance. Procedure 2: The section impedance obtained by Proc. 1 can be directly substituted into the calculation matrix (30) of concentric wires or composite wires (31).

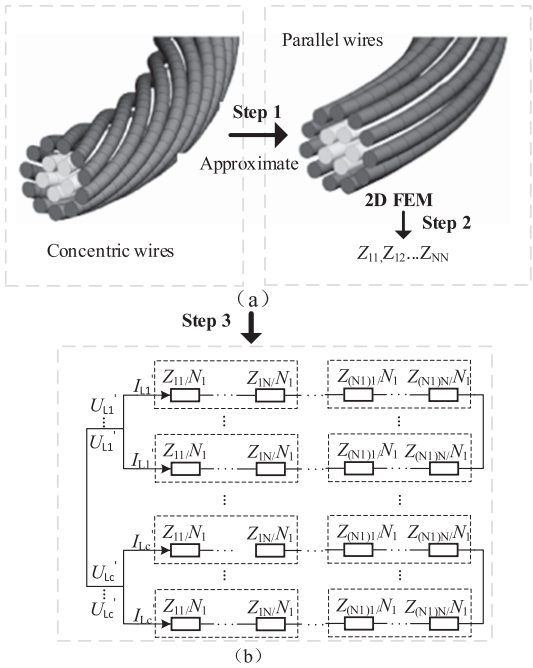

Fig. 3. Original SEC calculation method. (a) Segmented parallel wound wires are used to approximate concentric stranded litz wire. The impedance of parallel-wound wire is calculated using 2-D FEM. (b) Approximation can be represented as a circuit, where c is the number of layers of concentric strands, I_{Lc} is the current of the single strand in the cth layer, and N_c is the number of strands in the cth layer.

The twisting process of concentric litz wire involves twisting each single strand within each concentric layer around a common axis, resulting in a cylindrical shape. During this process, the cross-sectional view at any position does not change significantly, and the single wires in the same layer are constantly interchanging positions.

Thus, a segmented parallel wire can serve as a reasonable approximation for a concentric litz wire. In the SEC method, the impedance of each single wire in the concentric wires can be determined by averaging the impedances of all parallel wires within the same layer. This impedance is obtained by solving a 2-D FEM, as shown in Fig. 3(a). Similarly, the total voltage per single wire can be obtained by averaging the total voltage of all parallel wires in the same layer. This relationship is depicted in the circuit diagram shown in Fig. 3(b).

To summarize, original SEC uses a 2-D FEM to solve for the impedance of parallel-wound wires, and then substitutes the impedance into the equivalent circuit.

B. Simplification and Assumption

Two types of litz constructions are studied—concentric litz wire and composite litz wire, which can be seen in Fig. 1. This section begins by presenting the structures and application scenarios of two types of litz wire. Furthermore, a simplified geometry of their cross-sections is provided. Finally, the fundamental assumptions and limitations of iSEC are discussed.

Concentric wires are formed by simply twisting a small number of strands in one step, resulting in their interchanging within concentric circular arrangements. This initial twisting step is either part of a multiple twisting operation or the only twisting step for a litz wire composed of a small number of strands. When the number of strands satisfies the following equation [32], a single twisting operation is sufficient to avoid bundle-level skin effect

$$n_{1,\max} = \frac{4\delta^2}{d_w^2} \tag{1}$$

where δ is the skin depth for a solid conductor and d_w is the diameter of an individual strand. However, when the strand count exceeds $n_{1,\max}$, multiple stranding operations are required [32].

Based on our investigation, it has been found that litz wire manufacturers typically used the concentric structure, for litz wires containing up to 200 strands. However, for strand counts exceeding 200, a multiple-level twisting pattern, referred to as the composite stranding structure, is used to achieve a more stable configuration. Moreover, when the concentric layers exceed one, the strands are unable to interchange radial positions, resulting in an uneven current distribution. The composite wires, as discussed in this article, is considered as litz wires that achieve sufficient interchanging by employing suitable twisting patterns.

In terms of geometric structure, the strands of concentric wires interchanges only within their respective concentric layers. Specifically, as shown in Fig. 10(a), the inner layer consists of four strands, while the outer layer, represented by the blue shaded region, comprises 14 strands that interchange positions.

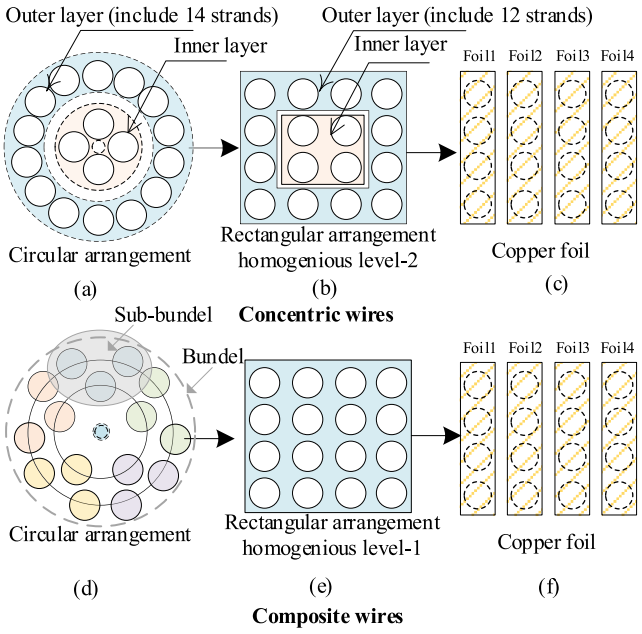

Fig. 4. Simplification of the litz wire shown in Fig. 1. (a) and (d) circular-arrangement strands. (b) and (e) simplified square arranged strands. (c) and (f) copper foil transformed from.

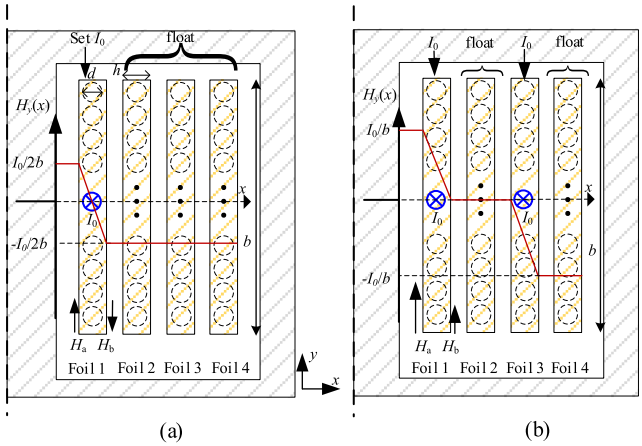

Fig. 5. Current conduction mode of copper foil. As a simple example to illustrate (3)–(5), $k_1 = 1$ and $k_2 = 3$. (a) Current mode 1 is used to calculate the self-resistance by setting one copper foil to peak current I_0. The other foils are set to float, i.e., no net current. (b) Current mode 2 is used to calculate the mutual resistance by setting two copper foils to peak current I_0. The rest of the copper foils are set to float. The circular dashed line represents the position of the strands before the transformation. Magnetic field distribution $Hy(x)$ is plotted with red line.

Conversely, in composite stranded cables, all 15 strands sequentially interchange positions throughout the cross-section [Fig. 4(d)]. To summarize, this article assumes limited regional conductor interchanges for concentric wires, whereas composite wires allow strands interchanges at any location.

To prepare for the iSEC calculation, the wire geometry is simplified. Fig. 4(a) shows two layers of a concentric wire, with 4 and 14 strands, respectively. The circular shape is converted into a 4×4 square-arrangement strands, and then transformed into 4 copper foils. For the composite wire in Fig. 4(d), the bundle is first converted into a 4×4 square arrangement based on the strand number, and then transformed into copper foils. In general, N_s strands are turned into a square arrangement of $N_r * N_r$ (N_r, N_s are positive integer), and then into N_r foils. Changes in quantity are corrected later.

It is important to emphasize that the simplification of N_r foil is used to calculate the impedance matrix of the rectangularly arranged strands shown in Fig. 4(b) and (e). It serves as an intermediate step and does not entirely replace litz wire with copper foil. The geometric structure of the rectangularly arranged strands will serve as the geometric basis for the interchanging method in the equivalent circuit, which will be introduced in Section III. The two types of litz wires exhibit distinct impedance characteristics due to their differing twisting patterns. Although both litz wires employ the same simplification approach, the different transposition matrix leads to varying equivalent impedance matrices, as illustrated in Fig. 1.

The following assumptions were used in the article.

1) The magnetic field varies slightly in the direction of the wire axis, so the section impedance matrix of each segment is constant. The difference in length of single strands within the litz wire is ignored.
2) The 1-D magnetic field is assumed in window.
3) Parasitic capacitance effect and displacement current are ignored [12], [13], [24], [27], [33], [34], [35].

The samples suitable for the approach should meet the following conditions.

1) The strands are regularly transposed within layers or sub-bundles, and the axial magnetic field of the litz wire does not vary significantly.
2) The 1-D field condition should be satisfied. Therefore, the winding height should almost occupy the window height and the winding layers are closed to each other. The magnetic permeability of the core should be high.
3) The approach is not applicable to very high frequency where capacitive effect is considerable. It is recommended to operate within the first resonance frequency to avoid significant capacitive effects.

C. Proc. 1.1: Calculation of the Resistance

In order to account for the active power coupling between the strands, the mutual resistance needs to be taken into consideration, as stated in [27]. The detailed principles for calculating the self and mutual resistance are described in [28].

Considering the effect of mutual resistance, the total power, averaged over one period of the sinusoidal excitation, of closed foils is

$$P = \frac{1}{2}\sum_{k=1}^{n} R_{kk}\,\dot{i}_k\,\dot{i}_k^* + \frac{1}{4}\sum_{k_1=1}^{n}\sum_{k_2=1}^{n} R_{k_1k_2}\left(\dot{i}_{k_1}\,\dot{i}_{k_2}^* + \dot{i}_{k_2}\,\dot{i}_{k_1}^*\right) \tag{2}$$

where $k_1 \neq k_2$, the "$*$" denotes conjugate of a complex current. Two current setting methods can be used to derive the self and mutual resistance by calculating the corresponding power as illustrated in Fig. 5.

For instance, when computing the self and mutual resistance of copper foils k_1 and k_2, one can apply a current amplitude I_0 to copper foil k_1, while keeping the other windings floating (i.e., with no net current), which results in

$$P_{11} = \frac{1}{2} R_{k1,k1} I_0^2 \tag{3}$$

where P_{11} represents the power of all foils. Similarly, applying the same conditions to copper foil k_2, it follows that

$$P_{22} = \frac{1}{2} R_{k2,k2} I_0^2. \tag{4}$$

Passing a current amplitude I_0 simultaneously to copper foil k_1, k_2 and floating the rest of the winding gives

$$P_{12} = \frac{1}{2} R_{k1,k1} I_0^2 + \frac{1}{2} R_{k2,k2} I_0^2 + R_{k1,k2} I_0^2. \tag{5}$$

Equations (3)–(5) contain three power unknowns, so the resistance can be calculated by obtaining the corresponding loss. The loss can be calculated from the magnetic fields on both sides of the foil [29]

$$\frac{P}{l} = \frac{1}{2} \frac{b\rho}{\delta} \left[(H_a - H_b)^2 \varsigma(h/\delta) + 2 H_a H_b \xi(h/\delta) \right] \tag{6}$$

$$\Delta = \frac{d_w}{\delta_w}, \delta = \sqrt{\frac{\rho_w}{\pi \mu f \gamma}}, \gamma = n_s \times N \times \frac{\pi d_w^2}{4bh}$$

$$\varsigma = \frac{\sinh(2\Delta) + \sin(2\Delta)}{\cosh(2\Delta) - \cos(2\Delta)}, \xi = \frac{\sinh \Delta - \sin \Delta}{\cosh \Delta + \cos \Delta} \tag{7}$$

where the field direction is ***y*** and varies only with ***x***. H_a and H_b are the boundary conditions for the ***x***-direction in a foil. The b and h are the width and thickness of the foil, respectively, γ is the filling factor, δ is the skin depth corrected for the filling factor, d_w is the single strand diameter, and N is the number of turns.

Thus, the power of (3) can be obtained from the magnetic field distribution in Fig. 5(a). Substituting H_a and H_b into (6) yields

$$P_{k1,k1} = \frac{b\rho}{2\delta} \left(\frac{I}{b} \right)^2 \left[\left(\varsigma(\Delta) + \frac{1}{2} \xi(\Delta) \right) l_{k1} + \frac{1}{2} \xi(\Delta) \sum_{k=1}^{n,k \neq k1} l_k \right]. \tag{8}$$

Substituting the expression into (3) for the self-resistance

$$R_{k1,k1} = \frac{2P}{|I_0|^2} = \frac{\rho}{\delta b} \left[\left(\varsigma(\Delta) + \frac{1}{2} \xi(\Delta) \right) l_{k1} + \frac{1}{2} \xi(\Delta) \sum_{k=1}^{n,k \neq k1} l_k \right]. \tag{9}$$

The mutual resistance can be obtained by combining (6) and the value from magnetic field boundary conditions of Fig. 5(b)

$$R_{k_1 k_2} = \frac{2P_{k1,k2} - I_0^2 (R_{k_1 k_1} + R_{k_2 k_2})}{2I_0^2} = \frac{\rho}{4\delta b} \left[2\varsigma(\Delta)(l_{k1} + l_{k2}) + 4\xi(\Delta) \left(\sum_{k=1}^{n} l_k - \sum_{k=k_1}^{k_2} l_k \right) - 2 \left(\varsigma(\Delta) + \frac{1}{2} \xi(\Delta) \right) (l_{k1} + l_{k2}) - \xi(\Delta) \left(2 \sum_{k=1}^{n} l_k - l_{k1} - l_{k2} \right) \right]$$

$$= \frac{\rho}{2\delta b} \xi(\Delta) \left(\sum_{k=1}^{n} l_k - 2 \sum_{k=k_1}^{k_2} l_k \right). \tag{10}$$

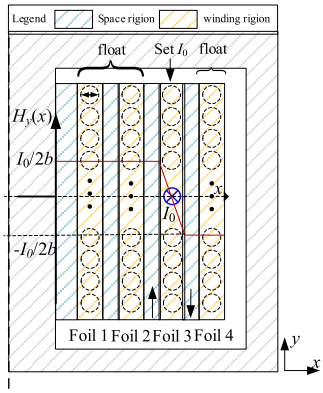

Fig. 6. Schematic diagram of winding magnetic field energy area.

The ac resistance of a single strand with N_1 turns can be derived from the relationship between the area of the copper foil and the single strand

$$R_{\text{strand}} = R_{\text{foil}} \frac{S_{\text{foil}} N_1}{S_{\text{cir}}}. \tag{11}$$

D. Proc. 1.2: Calculation of the Inductance

The matrix of inductance can be separated into two components: self-inductance and mutual inductance. The self-inductance can be determined through the relationship between inductance and magnetoresistance, which can be expressed as [30]

$$L = \frac{N\phi}{I} = \frac{N^2 B A_c}{H l_c} = \frac{N^2 \mu_r \mu_0 A_c}{l_c} = \frac{N^2}{\mathcal{R}} \tag{12}$$

where A_c and l_c refer to the average cross-sectional area and the average length of the magnetic circuit, respectively. Meanwhile, the mutual inductance can be deduced from the leakage energy between any two windings. Dowell [18] suggested dividing the energy interval into windings and spaces, as illustrated in Fig. 6. For instance, to calculate the mutual inductance between foils 1 and 3, a current of magnitude I_0 is applied to foil 3, and the field distribution is shown in Fig. 6. The energy stored in the space region can then be determined

$$W_m = \frac{1}{2} \int_V H \cdot B dv = \frac{\mu_0 I_0^2}{8b} l_w d_l \tag{13}$$

where d_l is the distance between the two windings and l_w is the average length of the winding. The expression for the magnetic field in the winding area is

$$H_y(x) = H_{\text{ext}} \frac{\sinh(\alpha x)}{\sinh(\alpha h)} - H_{\text{int}} \frac{\sinh(\alpha (x - h))}{\sinh(\alpha h)}$$

$$\alpha = \frac{1+j}{\delta}. \tag{14}$$

Then, the leakage energy in the winding area is

$$W_{m_w} = \frac{-\mu l_w b \delta}{16}\left(\frac{I_0}{b}\right)^2 \xi(\Delta). \tag{15}$$

The total leakage inductance is

$$L_\sigma = \frac{2W_l}{I_0^2} = \frac{\mu l_w d_l}{4b} - \frac{\mu l_w \delta}{8b}\xi(\Delta). \tag{16}$$

E. Proc. 1.3: Coefficient Modification

The process of converting strands to foils simplifies calculations, but it can introduce errors in the skin depth and magnetic field distribution. To address this issue, some researchers have proposed modifications to the penetration ratio Δ [19], [20]. For instance, in previous articles, a factor of $(\pi/4)^{3/4}$ was proposed by Wojda and Kazimierczuk [24] to account for the transformation of circular and rectangular conductors. This modification results in a decrease in the average current and magnetic field along the width direction of the winding by a factor of η. As a result, Ferreira suggested using η^2 to correct the proximity effect [19]. Then, (6) is rewritten as

$$\frac{P}{l} = \left(\frac{\pi}{4}\right)^{\left(\frac{3}{4}\right)} \frac{b\rho}{2\delta}\left[(H_a - H_b)\varsigma(h/\delta) + 2\eta^2 H_a H_b \xi(h/\delta)\right]. \tag{17}$$

In addition, as recalled in Fig. 4, the N_s strands are transformed into $N_r \times N_r$ strands, with N_r being a positive integer. Therefore, a modification for the number of strands is needed, affecting the skin depth and ac resistance. The dc resistance before and after transformation is equal

$$4\rho_w l_w / \left(\pi d^2 N n_r\right) = 4\rho_{wf} l_w / \left(\pi d^2 N \sqrt{N_s}\right) \tag{18}$$

which gives the ratio of two resistivities

$$\rho_w / \rho_{wf} = N_r / \sqrt{N_s}. \tag{19}$$

Hence, the ratio of the skin depths is given by

$$\delta_w / \delta_{wf} = \sqrt{N_r / \sqrt{N_s}}. \tag{20}$$

The effective skin depth is given by

$$\delta_p = \delta_w \sqrt{\frac{N_r}{\sqrt{N_s}}} = \delta \sqrt{\frac{N_r}{\gamma\sqrt{N_s}}}. \tag{21}$$

Thus, (17) was modified to

$$\frac{P}{l} = \left(\frac{\pi}{4}\right)^{\left(\frac{3}{4}\right)} \frac{b\rho}{2\delta}\sqrt{\frac{\gamma\sqrt{N_s}}{N_r}}\left[(H_a - H_b)\varsigma(\Delta_{wf}) + 2\eta^2 H_a H_b \xi(\Delta_{wf})\right]$$

$$\Delta_{wf} = \frac{h}{\delta}\sqrt{\frac{\gamma\sqrt{N_s}}{N_r}}. \tag{22}$$

The effect of the modification is compared in Fig. 7, where the ac resistance is shown using solid lines, and the bars represent the error in the average self-resistance. The absence of a modification would overestimate the eddy current effect, leading to errors in the ac resistance that increase with frequency. Therefore, a modification using a factor η in the equation is necessary.

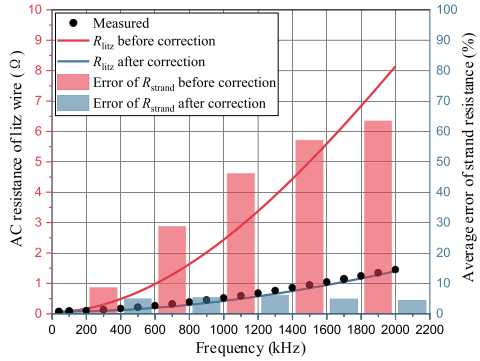

Fig. 7. Calculated and measured data for sample S1. The bars represent the single strand ac resistance error of the reference, and the details of the transformer parameters can be found in Table II.

III. Procedure 2: Circuit Derived Matrix

The twisting wires are considered as a cascade of circuits, which is shown in detail in subsection A. Further, in subsection B, the computational matrix for concentric and composite strands are derived based on the additional assumption and the impedance matrix derived in procedure 1.

A. Equivalent Circuit and Impedance Matrix

The equivalent circuit consists of section impedance as an element, which is connected according to the twisting pattern. Fig. 8 provides an example to illustrate the concept of section impedance. In Fig. 8, each section can be considered as a parallel strand. Thus, a twisted strand can be represented as a cascade of several parallel strands. Furthermore, the equivalent circuit can be represented as shown in Fig. 9. The gray shading indicates a section of strand. The value of section impedance is derived from procedure 1 and depends only on the position shown in Fig. 9. The voltage matrix consists of 16 strand-branches, represented by the column vectors $\boldsymbol{U}_{S1}$–$\boldsymbol{U}_{S16}$, with each containing the section voltage at different positions. For instance, $\boldsymbol{U}_{S1} = [U_{S1,1}\ U_{S1,2}\ U_{S1,3}\ \ldots\ U_{S1,16}]^T$, where $U_{S1,1}$ represents the voltage at position 1 of the first section.

The ***UI*** relationship for first section can be expressed as

$$\overset{(1)}{\begin{bmatrix} Z_{11} & Z_{12} & \cdot & Z_{1N} \\ Z_{21} & Z_{22} & \cdot & Z_{2\,\mathrm{N}} \\ \cdot & \cdot & \cdot & \cdot \\ Z_{16,1} & Z_{16,2} & \cdot & Z_{16,16} \end{bmatrix}} \begin{bmatrix} I'_1 \\ I'_2 \\ \ldots \\ I'_{16} \end{bmatrix} = \begin{bmatrix} U_{s1,1} \\ U_{s1,2} \\ \ldots \\ U_{s1,16} \end{bmatrix}. \tag{23}$$

As illustrated in Fig. 9, the branch currents vary with sections, which is represented by the multiplication of the ***T***-matrix. Furthermore, the ***UI*** relation for the kth section can be deduced

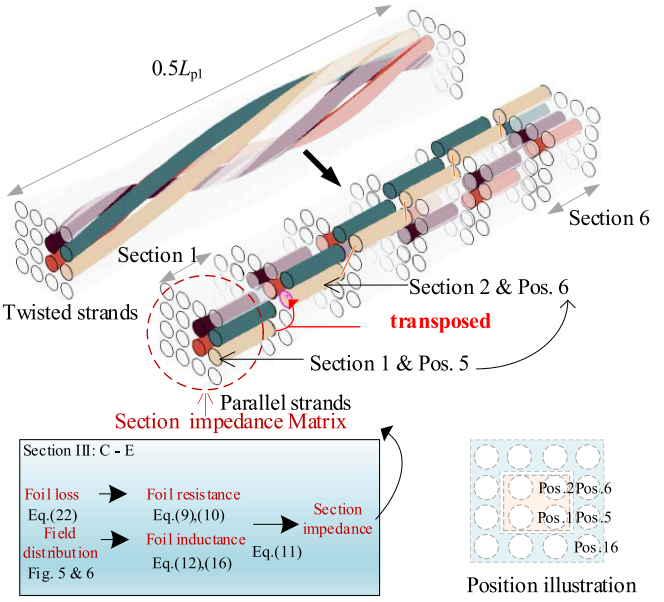

Fig. 8. Simplified process for twisting litz wire. The sections of the same color belong to the same strand. The inner layer of the litz wire contains 4 strands and the outer layer contains 12 strands. The pitch of the outer layer is Lp and that of the inner layer is $3Lp$, so that each strand is transposed at the same time. By dividing the strand in 1/12 Lp per sections, six sections can be obtained. Section impedance is obtained from procedure 1, as shown in the lower left block of the figure.

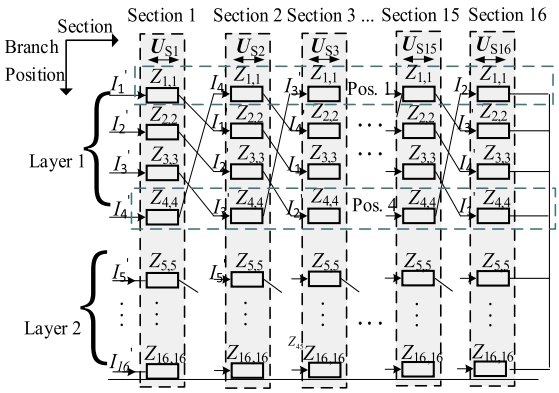

Fig. 9. Equivalent circuit of a 4∗4 arrangement of concentric litz wire. Section, position, and layer are important concepts that are often mentioned and are marked with gray shading, blue boxes, and brackets, respectively.

as

$$\overbrace{\begin{bmatrix} Z_{11} & Z_{12} & \cdot & Z_{1,16} \\ Z_{21} & Z_{22} & \cdot & Z_{2,16} \\ \cdot & \cdot & \cdot & \cdot \\ Z_{16,1} & Z_{16,2} & \cdot & Z_{16,16} \end{bmatrix}}^{\text{matrix for } k\text{thsection}} \boldsymbol{T}^{(k-1)} \overbrace{\begin{bmatrix} I'_1 \\ I'_2 \\ \cdots \\ I'_{16} \end{bmatrix}}^{\boldsymbol{I}_{sk}} = \overbrace{\begin{bmatrix} U_{sk,1} \\ U_{sk,2} \\ \cdots \\ U_{sk,16} \end{bmatrix}}^{\boldsymbol{U}sk}, \boldsymbol{T} = \begin{bmatrix} T_1 & 0 \\ 0 & T_2 \end{bmatrix}$$

$$\boldsymbol{T}_1 = \begin{bmatrix} \overbrace{\begin{matrix} 0 & 0 & 0 & 1 \\ 1 & 0 & 0 & 0 \\ 0 & 1 & 0 & 0 \\ 0 & 0 & 1 & 0 \end{matrix}}^{\text{positions of inner–layer}} \end{bmatrix},$$

$$\boldsymbol{T}_2 = \begin{bmatrix} \overbrace{\begin{matrix} 0 & .. & 0 & 1 \\ 1 & .. & 0 & 0 \\ .. & .. & .. & .. \\ 0 & .. & 1 & 0 \end{matrix}}^{\text{positions of outer–layer}} \end{bmatrix} \tag{24}$$

where the transposition matrix $\boldsymbol{T}_L$ ($L = 1$ or 2), a special Toeplitz matrix called as a circulant matrix, shifts the previous row vector's elements to the right and represents the transposition. The voltage of a single strand is the sum of all the section voltages. The strands are connected in parallel and the total voltage is expressed as a summation of voltages in each section

$$\boldsymbol{U}' = \sum_{k=1}^{12} \left(\boldsymbol{T}^{-1}\right)^{k-1} \boldsymbol{U}_{s_k}. \tag{25}$$

Substituting (25) to (24), the relationship between the single-strand current and voltage can be given as

$$\boldsymbol{U}' = \sum_{k=1}^{12} \left(\boldsymbol{T}^{-1}\right)^{(k-1)} \boldsymbol{Z}_{(k)} (\boldsymbol{T})^{(k-1)} \boldsymbol{I}' = Z_e \boldsymbol{I}' \tag{26}$$

where $\boldsymbol{Z}_{(k)}$ is the impedance matrix for kth section, and contains the section impedance for each position. $\boldsymbol{Z}_e$ denotes the equivalent impedance matrix for litz wire. The current of all strands of the litz wire can be calculated by (26).

B. Analytical Computing Matrix

Equation (26) requires the litz wire to be discreted into k sections in the axial direction, so it remains numerical. The summation times and order of matrix $\boldsymbol{T}$ are dependent on the number of strands. When there are a large number of strands, the solution could become overly burdensome.

To simplify (26), an additional precondition is defined that the field varies slightly in axial direction and the difference in length of single strands within the litz wire is ignored. The precondition results in a constant impedance matrix, denoted as $\boldsymbol{Z}_{(k)}$ in (26). As a result, only one calculation of the section impedance matrix is required. The impedance matrix $\boldsymbol{Z}_e$ in (26) should follow a specific form (see Appendix A for details), shown as follows:

$$\boldsymbol{Z}_e = \begin{bmatrix} \boldsymbol{S}_1 & \boldsymbol{M}_{12} \\ \boldsymbol{M}_{21} & \boldsymbol{S}_2 \end{bmatrix}$$

$$\boldsymbol{S}_A = \begin{bmatrix} sA_0 & sA_1 & sA_2 & sA_3 \\ sA_3 & sA_0 & sA_1 & sA_2 \\ sA_2 & sA_3 & sA_0 & sA_1 \\ sA_1 & sA_2 & sA_3 & sA_0 \end{bmatrix}$$

$$\boldsymbol{M}_{AB}=\begin{bmatrix} m_{AB,1} & m_{AB,2} & .. & m_{AB,4} \\ m_{AB,4} & m_{AB,1} & .. & m_{AB,3} \\ .. & .. & .. & .. \\ m_{AB,2} & m_{AB,3} & .. & m_{AB,1} \end{bmatrix}$$

$$\boldsymbol{M}_{BA}=\begin{bmatrix} m_{BA,1} & m_{BA,2} & .. & m_{BA,4} \\ m_{BA,4} & m_{BA,1} & .. & m_{BA,3} \\ .. & .. & .. & .. \\ m_{BA,2} & m_{BA,3} & .. & m_{BA,1} \end{bmatrix}$$

$$\boldsymbol{S}_{B}=\begin{bmatrix} sB_{.0} & sB_{1} & .. & sB_{11} \\ sB_{11} & sB_{0} & .. & sB_{10} \\ .. & .. & .. & .. \\ sB_{1} & sB_{2} & .. & sB_{0} \end{bmatrix} \tag{27}$$

where $\boldsymbol{S}_A$ and $\boldsymbol{S}_B$ are circulant matrices. $\boldsymbol{M}_{AB}$ and $\boldsymbol{M}_{BA}$ are partitioned circulant matrices that consist of circulant submatrices. Therefore, $\boldsymbol{Z}_e$ and $\boldsymbol{Z}_e{}^{-1}$ are partitioned circulant matrices as well (refer to Appendix B for detailed proof). As a result, the strand current matrix should have the following form:

$$\boldsymbol{I'}=\boldsymbol{Z}_e^{-1}\boldsymbol{U'}=\begin{bmatrix}\boldsymbol{K}_{11} & \boldsymbol{K}_{12}\\ \boldsymbol{K}_{21} & \boldsymbol{K}_{22}\end{bmatrix}\begin{bmatrix}uA'\\ uB'\end{bmatrix}=\begin{bmatrix}\boldsymbol{IA'}\\ \boldsymbol{IB'}\end{bmatrix}$$

$$\boldsymbol{uA'}=\overbrace{(u1..u1)^T}^{\text{inner-layer}},\boldsymbol{uB'}=\overbrace{(u2..u2)^T}^{\text{outer-layer}}$$

$$\boldsymbol{IA'}=\overbrace{(i1..i1)^T}^{\text{inner-layer}},\boldsymbol{IB'}=\overbrace{(i2..i2)^T}^{\text{outer-layer}} \tag{28}$$

where $\boldsymbol{Z}_e{}^{-1}$ is constructed using circulant matrices $\boldsymbol{K}_{11}$, $\boldsymbol{K}_{12}$, $\boldsymbol{K}_{21}$, and $\boldsymbol{K}_{22}$. The elements of the column vectors $\boldsymbol{I}_A$' and $\boldsymbol{I}_B$' are the same, respectively. Thereby there are two types of homogenous currents in the litz wire, which are distributed in layer 1 and layer 2, respectively, called two-level homogeneous current. For concentric wires, the strands of each layer have equal current based on the characteristics that the sum of elements in each row of the circulant matrix is equal, and that the strands are connected in parallel. Analogously, the $\boldsymbol{Z}_e$ matrix of the composite strand is a partitioned circulant matrix with one part (c.f. Appendix A), resulting in one homogeneous region. Based on these properties, two important conclusions can be derived as follows.

1) The strand currents of concentric wires in each layer are equal.
2) Each strand of the composite strand has an equal current.

These two conclusions reveal the most essential distinction and connection between concentric wires and composite wires. Specifically, when the number of layers is greater than 1, only partial regions of the concentric wires exhibit current homogeneity, while the composite ones achieve complete homogeneity. First, define the concept of homogeneous region, where the strand currents within the region are consistent. According to conclusion 1), the number of homogeneous regions in concentric strands is equal to the number of layers [c.f. Fig. 10(a)], whereas composite strands have only one homogeneous region [c.f. Fig. 10(c)]. As shown in Fig. 10(b), the homogeneous regions correspond to submatrices of the $\boldsymbol{T}$-matrix in (24). The characteristics of the homogeneous regions arise from the properties of

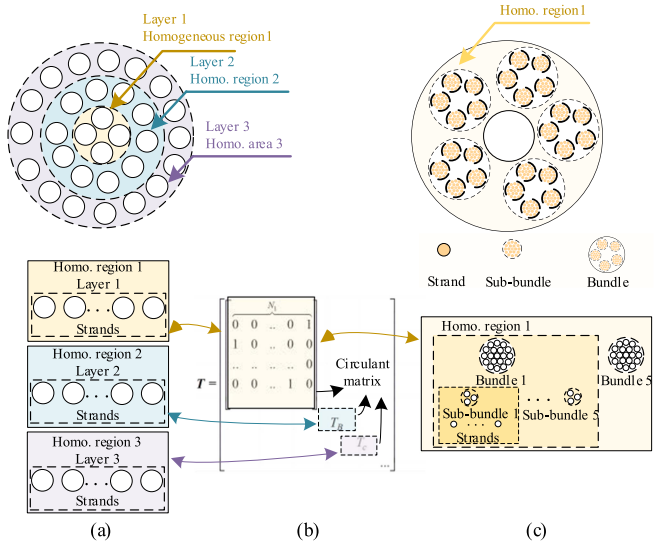

Fig. 10. Relationship between the homogeneous regions of concentric stranding and composite stranding in relation to the T matrix. (a) Concentric stranding, formed by a small number of strands through a single stranding operation, consists of three concentric layers, each forming a homogeneous region. (b) Transposition matrix $\boldsymbol{T}$ in (24), where each submatrix corresponds to a different homogeneous region and is a cyclic matrix. (c) Composite stranding, created by a large number of strands through multiple stranding operations, is considered to achieve uniform rearrangement under appropriate stranding patterns and possesses a single homogeneous region.

the $\boldsymbol{T}$-matrix: the corresponding submatrices within the $\boldsymbol{T}$-matrix are circulant matrices, as shown in Fig. 10(b). Moreover, when the number of layers in the concentric strands is 1, there is only one homogeneous region, and the $\boldsymbol{T}$-matrix becomes a circulant matrix. As a result, all strands achieve uniform current distribution.

Since the litz wire in this case (c.f. Fig. 8) has only two layers, there are only two strand currents. As a result, (26) can be simplified as

$$\begin{bmatrix}Z''_{11} & Z''_{12}\\ Z''_{21} & Z''_{22}\end{bmatrix}\begin{bmatrix}I''_1\\ I''_2\end{bmatrix}=\begin{bmatrix}U\\ U\end{bmatrix}$$

$$Z''_{11}=\frac{1}{4}\sum_{i=1}^{4}\sum_{j=1}^{4}S_A(i,j)=3\sum_{k_1=1}^{4}\sum_{k_2=1}^{4}Z'_{k_1,k_2}$$

$$=\frac{1}{4}\sum_{k_1=1}^{4}\sum_{k_2=1}^{4}Z'_{k_1,k_2}$$

$$Z''_{12}=\frac{1}{4}\sum_{i=1}^{4}\sum_{j=1}^{12}M_{AB}(i,j)=3\sum_{k_1=5}^{16}\sum_{k_2=1}^{4}Z'_{k_1,k_2}$$

$$=\frac{1}{4}\sum_{k_1=5}^{16}\sum_{k_2=1}^{4}Z_{k_1,k_2}$$

$$Z''_{21}=\frac{1}{12}\sum_{i=1}^{12}\sum_{j=1}^{4}M_{BA}(i,j)=\sum_{k_1=5}^{16}\sum_{k_2=1}^{4}Z'_{k_1,k_2}$$

$$=\frac{1}{12}\sum_{k_1=5}^{16}\sum_{k_2=1}^{4}Z_{k_1,k_2}$$

$$Z''_{22} = \frac{1}{12}\sum_{i=1}^{12}\sum_{j=1}^{12} S_A(i,j) = \left(\sum_{k_1=5}^{16}\sum_{k_2=5}^{16} Z'_{k_1,k_2}\right) = \frac{1}{12}\left(\sum_{k_1=5}^{16}\sum_{k_2=5}^{16} Z_{k_1,k_2}\right) \tag{29}$$

where $Z_{i,j} = Z'_{i,j} \times \lambda$, λ is the number of segments, I_1" and I_2" are the single strand current of the layers 1 and 2, respectively, and the total current is given by $I_{\text{sum}} = 4 \times I_1" + 12 \times I_2"$. Extending to the structure of c layers, where kth layer includes N_k strands, the ***UI*** equation is (30) shown at the bottom of this page.

From the above calculation, the equivalent impedance matrix of each layer can be derived. The diagonal elements are the self-impedance of the layer and the nondiagonal elements are the mutual impedance. The self-impedance characterizes the layer-level skin effect, and the mutual impedance represents the proximity effect.

The simplification of (30) reduces the order of matrix and the summation times compared to (26). It is useful for litz wires with a high number of strands

It is proved in Appendix A that the equivalent impedance matrix of a concentric strand is a partitioned circulant matrix, while the equivalent impedance matrix of a composite strand is a circulant matrix. This implies that concentric stranding can exhibit multiple homogeneous regions, whereas composite stranding has only one homogeneous region. From a computational perspective rather than a geometric one, the calculation method for composite stranding is a special case of concentric stranding. Specifically, in concentric litz wires with c layers, there are c different currents, whereas in composite wires, all strands have the same current. As a result, composite wires with N_s strands can be regarded as concentric wires with only one layer consisting of N_s strands. Bringing $c = 1$ into (30) yields

$$\frac{1}{N_s}\sum_{k_1=1}^{Ns}\sum_{k_2=1}^{Ns} Z_{k_1,k_2} I'' = U''. \tag{31}$$

Equations (30) and (31) provide a convenient calculation for concentric and composite wires, with no discrete required. The matrix elements are obtained from procedure 1. Therefore, it is full analytical. Moreover, litz wires where strands are transposed randomly can theoretically be calculated using (26) as long as the structure is known. However, such cases are beyond the scope of this article.

It is recommended to use (30) or (31) for calculating the ac resistance in instances where the length of the wires is much longer than the pitch of a single strand. Usually, the length of the litz wire is not an integral multiple of the pitch of the individual strands, resulting in partial transposition of strands over a certain length span. In contrast, (30) or (31) is used under the presumption of complete strand transposition within each homogeneous region. Consequently, under conditions where the length of the litz wires enables a sufficient transposition of strands within each homogeneous region, the resultant error arising from partial transposition remains minimal.

Using (30) and (31), the overall current of the litz wire is calculated, which then enables the calculation of the ac resistance. In a transformer, there are both primary and secondary sides, and thus the matrix contains the litz wire on both sides, shown as follows:

$$\begin{bmatrix} \overbrace{\cdots \quad \cdots}^{\text{Primary}} & \overbrace{\quad\quad}^{\text{Secondary}} \\ \cdots\ Z_{\beta p,\beta p} & \cdots\ Z_{\beta p+\beta u,\beta p+\beta u} \end{bmatrix} \begin{bmatrix} \overbrace{\cdots}^{\text{Pri.}} \\ I_{\beta p} \\ \overbrace{\cdots}^{\text{Sec.}} \\ I_{\beta p+\beta u} \end{bmatrix} = \begin{bmatrix} \overbrace{\cdots}^{\text{Pri.}} \\ U_{\beta p} \\ \overbrace{\cdots}^{\text{Sec.}} \\ U_{\beta p+\beta u} \end{bmatrix} \tag{32}$$

where $\beta_p = N_p \times C_p$, with N_p representing the number of parallel wire-branches on the primary side, and C_p denoting the number of layers in a single litz wire on the primary side as shown in Fig. 4(b) or (d), and $\beta_u = N_u \times C_u$ (N_u and C_u representing the corresponding values on the secondary side).

Take sample S1 of Table II as an example. The primary and secondary sides both have only one wire-branch, so N_p and N_u are 1. A total of 50 strands are transformed into a 7×7 square arrangement consisting of four concentric layers recalled in Fig. 4(b), so C_p and C_u are 4.

The short-circuit method is commonly used to calculate winding resistance. The winding impedance on primary side can be calculated through dividing the primary voltage by the primary

$$\begin{bmatrix} \frac{1}{N_1}\sum_{k_1=1}^{N_1}\sum_{k_2=1}^{N_1} Z_{k_1,k_2} & \frac{1}{N_1}\sum_{k_1=1}^{N_1}\sum_{k_2=N_1+1}^{N_1+N_2} Z_{k_1,k_2} & \cdots & \frac{1}{N_1}\sum_{k_1=1}^{N_1}\sum_{k_2=\sum_{k_3=1}^{c-1}N_{k_3}+1}^{Ns} Z_{k_1,k_2} \\ \frac{1}{N_2}\sum_{k_1=N_1+1}^{N_1+N_2}\sum_{k_2=1}^{N_1} Z_{k_1,k_2} & \frac{1}{N_2}\sum_{k_1=N_1+1}^{N_1+N_2}\sum_{k_2=N_1+1}^{N_1+N_2} Z_{k_1,k_2} & \cdots & \frac{1}{N_2}\sum_{k_1=N_1+1}^{N_1+N_2}\sum_{k_2=\sum_{k_3=1}^{c-1}N_{k_3}+1}^{Ns} Z_{k_1,k_2} \\ \vdots & \vdots & \cdots & \vdots \\ \frac{1}{N_c}\sum_{k_1=\sum_{k_3=1}^{c-1}N_{k_3}+1}^{Ns}\sum_{k_2=1}^{N_1} Z_{k_1,k_2} & \frac{1}{N_c}\sum_{k_1=\sum_{k_3=1}^{c-1}N_{k_3}+1}^{Ns}\sum_{k_2=N_1+1}^{N_1+N_2} Z_{k_1,k_2} & \cdots & \frac{1}{N_c}\sum_{k_1=\sum_{k_3=1}^{c-1}N_{k_3}+1}^{Ns}\sum_{k_2=\sum_{k_3=1}^{c-1}N_{k_3}+1}^{Ns} Z_{k_1,k_2} \end{bmatrix} \begin{bmatrix} I''_1 \\ I''_2 \\ \cdots \\ I''_c \end{bmatrix} = \begin{bmatrix} U''_1 \\ U''_2 \\ \cdots \\ U''_c \end{bmatrix}. \tag{30}$$

TABLE I
COMPUTING RECORD

Sample	Equation	CPU time (200 points)	Matrix-memory	Value (2 MHz)
S4	(26)	961 s	937 024 bytes	13.48
S4	(30) or (31)	2.4 s	2304 bytes	13.48
S8	(26)	3930 s	4 194 304 bytes	54.93
S8	(30) or (31)	23 s	64 bytes	54.93

current when the secondary side is short-circuited. In the matrix, set $U_{\beta p+1} - U_{\beta p+\beta s}$ to 0, which means that the secondary side is short-circuited

$$R_{\text{ac}} = \text{real}(Z_{\text{ac}}) = \text{real}\left(\frac{U_{\text{pri}}}{\sum_{k=1}^{\beta p} I_k}\right) \tag{33}$$

where U_{pri} is the voltage applied to the primary side. This equation represents the ac resistance referred to the primary side.

To demonstrate the effects of simplifications introduced in (30) and (31), we present the results of both methods in Table I for two samples. In order to ensure a fair comparison, we keep the value of $\boldsymbol{Z}_{(k)}$ constant when computing with (26). The sample parameters are shown in Table II. The CPU time represents the total time required to compute 200 frequency points ranging from 1 kHz to 2 MHz, while matrix memory indicates the memory space occupied by the impedance matrix in the equation. It is worth noting that when calculated using (31), the equivalent impedance matrix of composite strands has fewer orders and hence occupies less memory. However, the calculation time is longer compared to concentric wires due to the higher number of strands involved. The results indicate that the simplification leads to a significant reduction in CPU time and memory usage, by avoiding discrete elements and reducing the order of matrix, while maintaining the same accuracy as that of the discrete method, provided that the impedance matrix remains constant.

IV. RESULT AND DISCUSSION

A. Experimental and Measurement Setup

The experimental samples consisted of six types of litz wire, with a strand diameter of 0.1 mm, and varied in winding layers, cores, and number of turns. We obtained the winding resistance by shorting the secondary winding and measuring the impedance of the primary winding. In addition, we prepared 10 experimental samples (*S*1–*S*10) as detailed in Table II, with zinc ferrite LPC40 serving as the core material. Among these samples, 50, 120, and 150 strands were made of concentric wires, while the 250, 350, and 500 strands sample was composite ones. No air gap in the core for all samples. The geometric and computational assumptions are presented in Section II-B. We utilized the TONGHUI Impedance Analyzer TH2839 for testing, with the experimental setup displayed in Fig. 11.

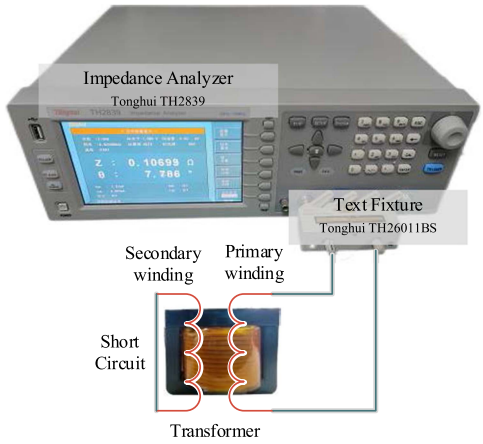

Fig. 11. Experimental instruments and methods.

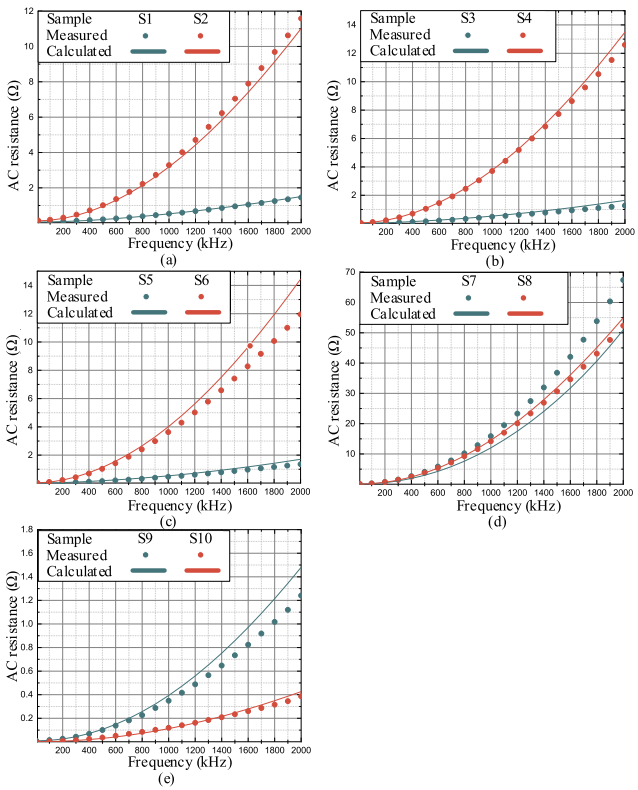

Fig. 12. Calculation results for iSEC and experimental results. Due to the capacitive effect, data within 2 MHz are shown.

B. Result and Discussion

We compared the experimental results with the analytical calculations to verify the accuracy of iSEC. As shown in Fig. 12(a)–(e), the average error was found to be 11.1% with the experimental data as the reference, indicating that iSEC agrees well with the experiments within the measured frequency scope. However, the error increases noticeably above 2 MHz, due to the fact that iSEC does not take into account the parasitic capacitance effect that occurs experimentally. Probably due to the lower resonant frequency, this error is larger in the samples with higher number of turns. Nevertheless, iSEC can meet the

TABLE II
EXPERIMENTAL SAMPLE PARAMETERS

Parameters	S1	S2	S3	S4	S5	S6	S7	S8	S9	S10
Strands number	50	50	120	120	150	150	150	250	350	500
Core type	EI33	EI33	EI50	EI50	EI50	EI50	EI60	EE80	EI70	EI40
Layer number	1	2	1	2	1	2	3	3	1	1
Turn number	17	34	13	26	12	24	39	30	9	5

TABLE III
COMPARATIVE DATA FOR THREE METHODS

	Adapt dowell	SFD	iSEC
Computing speed (ms)	3.7	3×10^3	408
Error (%)	19.2	18.78	11.1

usage requirements for common samples. This is because the operating frequency of transformers is typically lower than their first resonant frequency, which helps to avoid issues, such as port voltage spikes or current ringing, caused by resonant impedance. Additionally, considering that commonly used single strand diameters are larger than 0.05 mm, the operating frequency is generally below 2 MHz, which aligns with the intended range of application for iSEC.

The error of iSEC could be caused by several factors as follows.

1) The structure of the litz wire may deviate from the assumed concentric/complete transposition. Twisting imperfections can also add uncertainty to results [31].
2) The geometric simplification shown in Fig. 4 can introduce errors, which make it difficult to accurately calculate the mutual resistance between strands of the same layer.
3) The magnetic field may not fully satisfy the assumption of 1-D magnetic field.
4) HF capacitive effects is ignored.

Moreover, two classical calculating models for litz wire are compared, including, Adapt Dowell model [24] and the squared field derivative (SFD) [27]. Both methods are based on equal-current assumption. The error and computing speed are shown in Fig. 13 and Table III.

Generally, iSEC exhibits a small average error and a narrow interquartile range. In the calculation of concentric strands, it shows better results compared to SFD and adapt Dowell based on the equal-current assumption. It is due to the fact that samples 1–7 are based on concentric wires, where the current does not satisfy the assumption of uniform current distribution. Specifically, the SFD and adapt Dowell models show higher average errors for samples 1–7, with values of 21.3% and 21.67%, respectively. Conversely, the errors for samples 8–10, which are based on composite wires, are smaller, with values of 12.73% and 13.52%, respectively. Therefore, these two models based on the assumption of uniform current distribution exhibit larger errors in the multihomogeneous region. On the other hand, since iSEC can be applied to both multi- and single-homogeneous regions, its performance is relatively stable for both types of litz wires. The average computing speed of iSEC is between that of the formulaic adapt Dowell and the numerical SFD. This is mainly due to the higher order matrix resulting from more strands in iSEC. Nevertheless, iSEC can be applied reasonably for concentric and composite type litz wire.

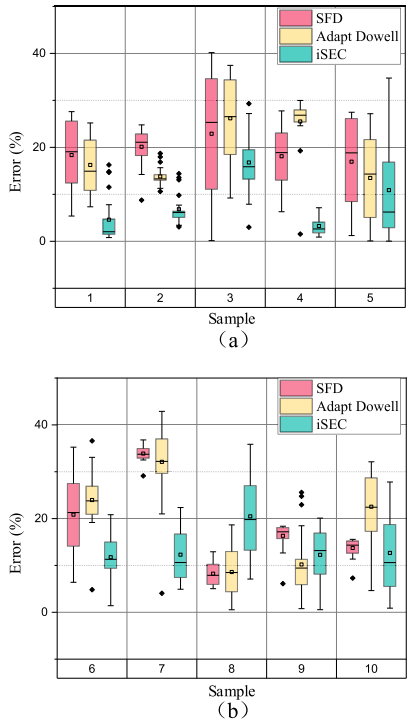

Fig. 13. Error box chart for SFD, adapt Dowell, and iSEC. The error is the average value within 2 MHz referenced to the experiment.

V. CONCLUSION

The iSEC proposed in this article is applicable to the ac resistance calculation of concentric and composite wires. The twisting process of litz wire is approximated as a cascade of multiple parallel strands, from which the calculation matrix is related to the twisting level, strand number, and number of discrete elements. It has been demonstrated that the equivalent impedance matrix is a circulant matrix, which ensures that the current is uniformly distributed within the layer of concentric strands, and the overall current is homogeneous in the composite strand, as long as the impedance matrix is constant for each section. Accordingly, a simplification is proposed by avoiding segmental discretization, through which the computational consumption is reduced significantly and the accuracy is maintained.

The section impedances are derived from the simplified geometry and 1-D magnetic field analysis. Physically based coefficient corrections are proposed to improve the computational accuracy by modifying errors introduced by the simplified geometry. In summary, the iSEC method is an ac resistance model that uses fully analytical calculations and with no discrete required. Referring to the experimental results of 10 transformer samples with different litz construction, winding layers, cores, and turns, the average computing error in studied cases of iSEC is 11.1% within 2 MHz.

APPENDIX

A. *Mathematical Proof of the Partitioned-Circulant Property of the Equivalent Impedance Matrix*

Without loss of generality, the concentric strands, consisting of c layers with N_k strands in the kth layer, are studied. The number of segments $\lambda = \Pi(N_1 \ldots N_c)$. Equation (26) can be rewritten as

$$\boldsymbol{U}' = \sum_{k=1}^{\lambda} \left(\boldsymbol{T}^{-1}\right)^{(k-1)} \boldsymbol{Z}_{(k)} (\boldsymbol{T})^{(k-1)} \boldsymbol{I}' = \boldsymbol{Z}_e \boldsymbol{I}'$$

$$= \sum_{k=1}^{\lambda} \boldsymbol{Z'}_{(\boldsymbol{k})} \boldsymbol{I}' = \begin{bmatrix} \overbrace{\boldsymbol{S}_1}^{N1} & \overbrace{\boldsymbol{M}_{12}}^{N2} & .. & \overbrace{\boldsymbol{M}_{1C}}^{Nc} \\ \boldsymbol{M}_{21} & \boldsymbol{S}_2 & .. & \boldsymbol{M}_{2C} \\ .. & .. & .. & .. \\ \boldsymbol{M}_{C1} & \boldsymbol{M}_{C2} & .. & \boldsymbol{S}_C \end{bmatrix} \boldsymbol{I}'$$

$$\boldsymbol{T} = \begin{bmatrix} \boldsymbol{T}_A & & & \\ & \boldsymbol{T}_B & & \\ & & .. & \\ & & & \boldsymbol{T}_C \end{bmatrix}, \boldsymbol{T}_C = \begin{bmatrix} \overbrace{\begin{matrix} 0 & 0 & .. & 0 & 1 \\ 1 & 0 & .. & 0 & 0 \\ .. & .. & .. & .. & 0 \\ 0 & 0 & .. & 1 & 0 \end{matrix}}^{Nc} \\ \\ \end{bmatrix} \quad (34)$$

where $\boldsymbol{Z'}_{(k)}$ is the section impedance matrix of the kth segment, which contains the section impedance of each strand. The $\boldsymbol{S}$ and $\boldsymbol{M}$ matrices are submatrices of the impedance matrix, with their dimensions determined by the number of strands in a specific layer. In the following section, we will demonstrate the properties of the impedance matrix by utilizing the patterns observed in the $\boldsymbol{S}$ and $\boldsymbol{M}$ matrices. According to (34), the expression of $\boldsymbol{Z'}_{(k)}$ is

$$\boldsymbol{Z'_{(k)}} = \left(\boldsymbol{T}^{-1}\right)^{(k-1)} \begin{bmatrix} \overbrace{\boldsymbol{S}_{(\boldsymbol{k})1}}^{N_1} & \overbrace{\boldsymbol{M}_{(\boldsymbol{k})12}}^{N_2} & .. & \overbrace{\boldsymbol{M}_{(\boldsymbol{k})1\,C}}^{N_c} \\ \boldsymbol{M}_{(\boldsymbol{k})21} & \boldsymbol{S}_{2(\boldsymbol{k})} & .. & \boldsymbol{M}_{(\boldsymbol{k})2\,C} \\ .. & .. & .. & .. \\ \boldsymbol{M}_{(\boldsymbol{k})C1} & \boldsymbol{M}_{(\boldsymbol{k})C2} & .. & \boldsymbol{S}_{(\boldsymbol{k})C} \end{bmatrix} (\boldsymbol{T})^{(k-1)} \quad (35)$$

where the submatrices $\boldsymbol{S}_{(k)i}$ and $\boldsymbol{M}_{(k)ij}$ are derived from the impedance matrix $\boldsymbol{Z}_{(k)}$, and their dimensions are determined by the number of strands in a specific layer. E.g., the expressions for $\boldsymbol{S_{(k)}}_1$ and $\boldsymbol{M_{(k)}}_{12}$ are given as

$$\boldsymbol{S}_{(\boldsymbol{k})1} = \begin{bmatrix} \overset{k}{s}_{1,1} & .. & .. & \overset{k}{s}_{1,j} & \cdots \\ .. & .. & .. & .. & .. \\ & & \overset{k}{s}_{i,j} & & \\ & & & \overset{k}{s}_{i+1,j+1} & \\ & & & & \cdots \end{bmatrix}$$

$$\boldsymbol{S}_1(\mathrm{i},\mathrm{j}) = \sum_{k=1}^{\lambda} \overset{k}{s}_{ij}, \lambda = \prod_{k=1}^{C} N_k$$

$$\overset{k}{s}_{i,j} = \boldsymbol{Z'}(1 + \mathrm{rem}(i-2+k, N_1), 1 + \mathrm{rem}(j-2+k, N_1)) \quad (36)$$

where the term rem (k, N_1) represents the remainder of k divided by N_1, which indicates that the strand position (i.e., the lower corner mark) can only be shifted within a specific range. Using this concept, the relationship of the elements in the $\boldsymbol{S}_1$ matrix on the parallel lines of the diagonal can be deduced as

$$\boldsymbol{S}_1(i+1, j+1) = \sum_{k=1}^{\lambda} \overset{k}{s}_{i+1,j+1} = \sum_{k=1}^{\lambda} \overset{k+1}{s}_{i,j} = \boldsymbol{S}_1(i,j)$$

$$\boldsymbol{S}_1(i+1, 1) = \sum_{k=1}^{\lambda} \overset{k}{s}_{i+1,1}$$

$$= \sum_{k=1}^{\lambda} \boldsymbol{Z'}(1 + \mathrm{rem}(i+k-1, N_1), 1 + \mathrm{rem}(k-1, N_1))$$

$$= Z_{i+1,1} + \ldots + Z_{i+\lambda,\lambda}$$

$$= Z_{i,N1} + Z_{i+1,1} + Z_{i+2,2} + \ldots$$

$$= \boldsymbol{S}_1(i, N_1). \quad (37)$$

The equation above indicates that a particular row element of matrix S1 is obtained by shifting the elements of the previous row one position to the right. Therefore, $\boldsymbol{S}_1$ is a circulant matrix. $\boldsymbol{M}_{12}$ can be represent as

$$\boldsymbol{M}_{(\boldsymbol{k})12} = \begin{bmatrix} \overset{k}{m}_{1,1} & .. & .. & \overset{k}{m}_{1,j} & \cdots \\ .. & .. & .. & .. & .. \\ & & \overset{k}{m}_{i,j} & & \\ & & & \overset{k}{m}_{i+1,j+1} & \\ & & & & \cdots \end{bmatrix}$$

$$\overset{k}{m}_{i,j} = \boldsymbol{Z'}(1 + \mathrm{rem}(i-2+k, N_1), N_1 + 1 + \mathrm{rem}(j-2+k, N_2))$$

$$\boldsymbol{M}_{12}(\mathrm{i},\mathrm{j}) = \sum_{k=1}^{\lambda} \overset{k}{m}_{ij} = \left(\prod_{k=1}^{C, k\neq 1, k\neq 2} N_k\right) \sum_{k1=1}^{N1,} \left(\sum_{k2=N1+1}^{N1+N2} Z_{k1,k2}\right). \quad (38)$$

Accordingly, the elements of $\boldsymbol{M}_{12}$ are equal. Note that a sufficient condition for this conclusion to hold is that $\lambda = \Pi(N_1 \ldots N_k)$. Generalizing (37) and (38), the expression for any submatrix element of the $\boldsymbol{Z}$ matrix is given as

$$\begin{aligned}
&{}^{k}_{s_{i,j}} = \boldsymbol{Z'}(g(m) + \mathrm{rem}(i-2+k, N_m), g(m) \\
&\qquad + \mathrm{rem}(j-2+k, N_m)) \\
&{}^{k}_{m_{i,j}} = \boldsymbol{Z'}(g(m) + \mathrm{rem}(i-2+k, N_m), g(n) \\
&\qquad + \mathrm{rem}(j-2+k, N_n)) \\
&g(x) = \sum_{x=1}^{x-1} N_x + 1, N_0 = 0 \\
&\boldsymbol{M}_{mn}(\mathrm{i},\mathrm{j}) = \sum_{k=1}^{\lambda} {}^{k}_{m_{ij}} \\
&\quad = \left(\prod_{k=1}^{C,k\neq m,k\neq m} N_k \right) \sum_{k1=g(m)}^{g(m)+Nm-1,} \left(\sum_{k2=g(n)}^{g(n)+Nn-1} Z_{k1,k2} \right).
\end{aligned} \tag{39}$$

Due to the arbitrariness of $\boldsymbol{S}_m$ and $\boldsymbol{M}_{mn}$, both diagonal part and nondiagonal part of $\boldsymbol{Z}_e$ are circulant matrix. Therefore, $\boldsymbol{Z}_e$ is a partitioned circulant matrix.

It is worth explaining, the λ in (26) is the least common multiple of 4 and 2, which is less than 4×12, so the elements are not equal everywhere. Nevertheless, ${\boldsymbol{Z}_e}^{-1}$ in (28) is still a partitioned circulant matrix.

The proof of the equivalent impedance matrix for the composite stranded wire is similar to that of the concentric wire. For a composite stranded wire with N_s strands, the structure is considered to be ideally designed to allow the strands to be transposed sequentially at all positions. Then, (34) can be rewritten as

$$\begin{aligned}
&\boldsymbol{U'} = \sum_{k=1}^{Ns} \left(\boldsymbol{T_L}^{-1}\right)^{(k-1)} \boldsymbol{Z}_{(k)} \left(\boldsymbol{T_L}\right)^{(k-1)} \boldsymbol{I'} = \boldsymbol{Z}_e \boldsymbol{I'} \\
&\boldsymbol{T_L} = \begin{bmatrix} \overbrace{\begin{matrix} 0 & 0 & .. & 0 & 1 \\ 1 & 0 & .. & 0 & 0 \\ .. & .. & .. & .. & .. \\ 0 & 0 & .. & 1 & 0 \end{matrix}}^{Ns} \\ \\ \end{bmatrix}
\end{aligned} \tag{40}$$

where $\boldsymbol{T}_L$ is a submatrix of the transposition matrix in (34), so the proof of $\boldsymbol{Z}_e$ is similar to that of the matrix $\boldsymbol{S}$ and $\boldsymbol{M}$ in (37) and (38). As a result, $\boldsymbol{Z}_e$ is a circulant matrix.

B. Mathematical Proof of the Properties of Partitioned Circulant Matrix

The inverse matrix of a partitioned circulant matrix is also a partitioned circulant matrix. This conclusion is proved by three properties as follows.

Property 1: If the submatrix of partitioned matrix $\boldsymbol{H}$ is of the diagonal matrix, then $\boldsymbol{H}^{-1}$ is also a partitioned matrix, whose submatrix is diagonal matrix

$$[\boldsymbol{H}\,|\boldsymbol{E}] = \left[\begin{array}{cccc|cccc} \boldsymbol{\Lambda}_{11} & \boldsymbol{\Lambda}_{12} & .. & \boldsymbol{\Lambda}_{1c} & \boldsymbol{E}_{11} & & & \\ \boldsymbol{\Lambda}_{21} & \boldsymbol{\Lambda}_{22} & .. & \boldsymbol{\Lambda}_{2c} & & \boldsymbol{E}_{22} & & \\ .. & .. & .. & .. & & & \cdots & \\ \boldsymbol{\Lambda}_{c1} & \boldsymbol{\Lambda}_{c2} & .. & \boldsymbol{\Lambda}_{cc} & & & & \boldsymbol{E}_{cc} \end{array}\right]. \tag{41}$$

After the left half transformed into an identity matrix by elementary operation, the submatrix of the right half should be a diagonal matrix. This is because the sum and the product of diagonal matrix are still diagonal matrix. Therefore, $\boldsymbol{H}^{-1}$ is also a matrix of partitioned matrix, whose submatrix is diagonal matrix.

Property 2: Define:

$$\boldsymbol{A} = \begin{bmatrix} a_1 & a_2 & a_3 & .. & a_n \\ a_n & a_1 & a_2 & .. & a_{n-1} \\ .. & .. & & .. & .. \\ a_2 & a_3 & a_4 & .. & a_1 \end{bmatrix}. \tag{42}$$

Suppose:

$$\begin{aligned}
f(x) &= a_1 + a_2 x + \ldots + a_n x^{n-1} \\
\omega_k &= \cos\frac{2k\pi}{n} + i\sin\frac{2k\pi}{n} \\
k &= 0, 1, \ldots, n-1.
\end{aligned} \tag{43}$$

The following equation is derived:

$$\begin{bmatrix} a_1 & a_2 & a_3 & .. & a_n \\ a_n & a_1 & a_2 & .. & a_{n-1} \\ .. & .. & & .. & .. \\ a_2 & a_3 & a_4 & .. & a_1 \end{bmatrix} \begin{bmatrix} 1 \\ \omega_k \\ .. \\ \omega_k^{n-1} \end{bmatrix} = f(\omega_k) \begin{bmatrix} 1 \\ \omega_k \\ .. \\ \omega_k^{n-1} \end{bmatrix}. \tag{44}$$

It shows that $(1,\omega_k, \ldots, {\omega_k}^{n-1})^T$ is an eigenvector of $\boldsymbol{A}$ belonging to the eigenvalue $f(\omega_k)$.

Define the matrix $\boldsymbol{N}$ as follows:

$$\begin{aligned}
\boldsymbol{N} &= \begin{bmatrix} 1 & 1 & \ldots & 1 \\ 1 & \omega_1 & \ldots & \omega_{(n-1)} \\ 1 & \ldots & \ldots & \ldots \\ 1 & \omega_1^{n-1} & \ldots & \omega_{(n-1)}^{(n-1)} \end{bmatrix} \\
\omega_k &= \cos\frac{2k\pi}{n} + i\sin\frac{2k\pi}{n} (0 \le k \le n-1).
\end{aligned} \tag{45}$$

According to the Vander Monde determinant, it is known that $|\boldsymbol{N}| \neq 0$, so the n eigenvectors are linearly independent.

Then the sufficient and necessary condition for $\boldsymbol{A}$ to be a circulant matrix is that: there exists a diagonal matrix Λ such that $\boldsymbol{A} = \boldsymbol{N}\Lambda\boldsymbol{N}^{-1}$.

Property 3: Sufficient and necessary condition for $\boldsymbol{Z}$ to be a partitioned circulant matrix is that there exists a partitioned matrix $\boldsymbol{H}$ whose submatrix is a diagonal matrix such that $\boldsymbol{Z} = \boldsymbol{PHP}^{-1}$.

According to property 2, $\boldsymbol{Z}$ can be expressed as

$$\begin{aligned}\boldsymbol{Z} &= \begin{bmatrix} \overbrace{\boldsymbol{S}_A}^{N_1} & \overbrace{\boldsymbol{M}_{A,B}}^{N_2} & .. & \overbrace{\boldsymbol{M}_{A,\,C}}^{N_c} \\ \boldsymbol{M}_{B,A} & \boldsymbol{S}_B & .. & \boldsymbol{M}_{B,\,C} \\ .. & .. & .. & .. \\ \boldsymbol{M}_{C,A} & \boldsymbol{M}_{C,B} & .. & \boldsymbol{S}_C \end{bmatrix} \\ &= \begin{bmatrix} \boldsymbol{N}\boldsymbol{\Lambda}_{11}\boldsymbol{N}^{-1} & \boldsymbol{N}\boldsymbol{\Lambda}_{12}\boldsymbol{N}^{-1} & .. & \boldsymbol{N}\boldsymbol{\Lambda}_{1c}\boldsymbol{N}^{-1} \\ \boldsymbol{N}\boldsymbol{\Lambda}_{21}\boldsymbol{N}^{-1} & \boldsymbol{N}\boldsymbol{\Lambda}_{22}\boldsymbol{N}^{-1} & .. & \boldsymbol{N}\boldsymbol{\Lambda}_{2c}\boldsymbol{N}^{-1} \\ .. & .. & .. & .. \\ \boldsymbol{N}\boldsymbol{\Lambda}_{c1}\boldsymbol{N}^{-1} & \boldsymbol{N}\boldsymbol{\Lambda}_{c2}\boldsymbol{N}^{-1} & .. & \boldsymbol{N}\boldsymbol{\Lambda}_{cc}\boldsymbol{N}^{-1} \end{bmatrix} \\ &= \begin{bmatrix} \boldsymbol{N} & & & \\ & \boldsymbol{N} & & \\ & & \cdots & \\ & & & \boldsymbol{N} \end{bmatrix} \begin{bmatrix} \boldsymbol{\Lambda}_{11} & \boldsymbol{\Lambda}_{12} & .. & \boldsymbol{\Lambda}_{1c} \\ \boldsymbol{\Lambda}_{21} & \boldsymbol{\Lambda}_{22} & .. & \boldsymbol{\Lambda}_{2c} \\ .. & .. & .. & .. \\ \boldsymbol{\Lambda}_{c1} & \boldsymbol{\Lambda}_{c2} & .. & \boldsymbol{\Lambda}_{cc} \end{bmatrix} \\ &\quad \times \begin{bmatrix} \boldsymbol{N} & & & \\ & \boldsymbol{N} & & \\ & & \cdots & \\ & & & \boldsymbol{N} \end{bmatrix} \\ &= \boldsymbol{P}\boldsymbol{H}\boldsymbol{P}^{-1}. \end{aligned} \tag{46}$$

Suppose there exists $\boldsymbol{H}$ as

$$\boldsymbol{H} = \begin{bmatrix} \boldsymbol{\Lambda}_{11} & \boldsymbol{\Lambda}_{12} & .. & \boldsymbol{\Lambda}_{1c} \\ \boldsymbol{\Lambda}_{21} & \boldsymbol{\Lambda}_{22} & .. & \boldsymbol{\Lambda}_{2c} \\ .. & .. & .. & .. \\ \boldsymbol{\Lambda}_{c1} & \boldsymbol{\Lambda}_{c2} & .. & \boldsymbol{\Lambda}_{cc} \end{bmatrix} \tag{47}$$

where $\boldsymbol{\Lambda}$ is the diagonal matrix. Further, $\boldsymbol{Z} = \boldsymbol{P}\boldsymbol{H}\boldsymbol{P}^{-1}$, which yields

$$\begin{aligned}\boldsymbol{P}\boldsymbol{H}\boldsymbol{P}^{-1} &= \begin{bmatrix} \boldsymbol{N} & & & \\ & \boldsymbol{N} & & \\ & & \cdots & \\ & & & \boldsymbol{N} \end{bmatrix} \begin{bmatrix} \boldsymbol{\Lambda}_{11} & \boldsymbol{\Lambda}_{12} & .. & \boldsymbol{\Lambda}_{1c} \\ \boldsymbol{\Lambda}_{21} & \boldsymbol{\Lambda}_{22} & .. & \boldsymbol{\Lambda}_{2c} \\ .. & .. & .. & .. \\ \boldsymbol{\Lambda}_{c1} & \boldsymbol{\Lambda}_{c2} & .. & \boldsymbol{\Lambda}_{cc} \end{bmatrix} \\ &\quad \begin{bmatrix} \boldsymbol{N} & & & \\ & \boldsymbol{N} & & \\ & & \cdots & \\ & & & \boldsymbol{N} \end{bmatrix}^{-1} \\ &= \begin{bmatrix} \boldsymbol{N}\boldsymbol{\Lambda}_{11}\boldsymbol{N}^{-1} & \boldsymbol{N}\boldsymbol{\Lambda}_{12}\boldsymbol{N}^{-1} & .. & \boldsymbol{N}\boldsymbol{\Lambda}_{1c}\boldsymbol{N}^{-1} \\ \boldsymbol{N}\boldsymbol{\Lambda}_{21}\boldsymbol{N}^{-1} & \boldsymbol{N}\boldsymbol{\Lambda}_{22}\boldsymbol{N}^{-1} & .. & \boldsymbol{N}\boldsymbol{\Lambda}_{2c}\boldsymbol{N}^{-1} \\ .. & .. & .. & .. \\ \boldsymbol{N}\boldsymbol{\Lambda}_{c1}\boldsymbol{N}^{-1} & \boldsymbol{N}\boldsymbol{\Lambda}_{c2}\boldsymbol{N}^{-1} & .. & \boldsymbol{N}\boldsymbol{\Lambda}_{cc}\boldsymbol{N}^{-1} \end{bmatrix}. \end{aligned} \tag{48}$$

According to property 3, $\boldsymbol{P}$ is a partitioned circulant matrix. Therefore, the inverse matrix of $\boldsymbol{Z}$ can be expressed as

$$\boldsymbol{Z}^{-1} = \left(\boldsymbol{P}\boldsymbol{H}\boldsymbol{P}^{-1}\right)^{-1} = \boldsymbol{P}\boldsymbol{H}^{-1}\boldsymbol{P}^{-1}. \tag{49}$$

Based on property 1, $\boldsymbol{H}^{-1}$ is also a partitioned matrix whose submatrix is a diagonal matrix. Further, according to property 3, $\boldsymbol{Z}^{-1}$ is a partitioned circulant matrix.

REFERENCES

[1] K. Strunz, E. Abbasi, and D. N. Huu, "DC microgrid for wind and solar power integration," *IEEE J. Emerg. Sel. Topics Power Electron.*, vol. 2, no. 1, pp. 115–126, Mar. 2014.

[2] D. K. Mishra et al., "A review on solid-state transformer: A breakthrough technology for future smart distribution grids," *Int. J. Elect. Power*, vol. 133, Dec. 2021, Art. no. 107255.

[3] M. R. Islam, Y. G. Guo, and J. G. Zhu, "A review of offshore wind turbine nacelle: Technical challenges, and research and developmental trends," *Renewable Sustain. Energy Rev.*, vol. 33, pp. 161–176, May 2014.

[4] Z. C. Guo, R. Y. Yu, W. Xu, X. Y. Feng, and A. Q. Huang, "Design and optimization of a 200-kW medium-frequency transformer for medium-voltage SiC PV inverters," *IEEE Trans. Power Electron.*, vol. 36, no. 9, pp. 10548–10560, Sep. 2021.

[5] J. E. Huber and J. W. Kolar, "Applicability of solid-state transformers in today's and future distribution grids," *IEEE Trans. Smart Grid*, vol. 10, no. 1 pp. 317–326, Jan. 2019.

[6] M. Mogorovic and D. Dujic, "100 kW, 10 kHz medium-frequency transformer design optimization and experimental verification," *IEEE Trans. Power Electron.*, vol. 34, no. 2 pp. 1696–1708, Feb. 2019.

[7] T. O. Olowu, H. Jafari, M. Moghaddami, and A. I. Sarwat, "Multiphysics and multiobjective design optimization of high-frequency transformers for solid-state transformer applications," *IEEE Trans. Ind. Appl.*, vol. 57, no. 1, pp. 1014–1023, Jan./Feb. 2021.

[8] J. Acero, I. Lope, J. M. Burdio, C. Carretero, and R. Alonso, "Loss analysis of multistranded twisted wires by using 3D-FEA simulation," in *Proc. IEEE 15th Workshop Control Model. Power Electron.*, 2014, pp. 1–6.

[9] D. Lin, C. Lu, N. Chen, and P. Zhou, "An efficient method for litz-wire AC loss computation in transient finite element analysis," *IEEE Trans. Magn.*, vol. 58, no. 5, May 2022, Art. no. 7400710.

[10] A. Delgado, G. Salinas, J. A. Oliver, J. A. Cobos, and J. Rodriguez-Moreno, "Equivalent conductor layer for fast 3-D finite element simulations of inductive power transfer coils," *IEEE Trans. Power Electron.*, vol. 35, no. 6, pp. 6221–6230, Jun. 2020.

[11] A. E. Ruehli and P. A. Brennan, "Efficient capacitance calculations for three-dimensional multiconductor systems," *IEEE Trans. Microw. Theory Techn.*, vol. MTT-21, no. 2, pp. 76–82, Feb. 1973.

[12] S. Ehrlich, H. Rossmanith, M. Sauer, C. Joffe, and M. März, "Fast numerical power loss calculation for high-frequency litz wires," *IEEE Trans. Power Electron.*, vol. 36, no. 2, pp. 2018–2032, Feb. 2021.

[13] A. Rosskopf and C. Brunner, "Enhancing litz wire power loss calculations by combining a sparse strand element equivalent circuit method with a Voronoi-based geometry model," *IEEE Trans. Power Electron.*, vol. 37, no. 9, pp. 11450–11456, Sep. 2022.

[14] B. Jurisic, I. Uglesic, A. Xemard, and F. Paladian, "Difficulties in high frequency transformer modeling," *Elect. Power Syst. Res.*, vol. 138, pp. 25–32, Sep. 2016.

[15] B. Chen and L. Lin, "Semi-empirical model for precise analysis of copper losses in high-frequency transformers," *IEEE Access*, vol. 6, pp. 3655–3667, 2018.

[16] M. Mogorovic and D. Dujic, "FEM-based statistical data-driven modeling approach for MFT design optimization," *IEEE Trans. Power Electron.*, vol. 35, no. 10, pp. 10863–10872, Oct. 2020.

[17] J. Li, W. Water, B. Y. Zhu, and J. W. Lu, "Integrated high-frequency coaxial transformer design platform using artificial neural network optimization and FEM simulation," *IEEE Trans. Mag.*, vol. 51, no. 3, Mar. 2015, Art. no. 8400204.

[18] P. L. Dowell, "Effect of eddy currents in transformer windings," *Proc. Inst. Elect. Eng.*, vol. 113, no. 8, pp. 1387–1394, Aug. 1966.

[19] J. Ferreira, "Appropriate modelling of conductive losses in the design of magnetic components," in *Proc. IEEE Power Electron. Specialist Conf.*, 1990, pp. 780–785.

[20] F. Robert, "A theoretical discussion about the layer copper factor used in winding loss calculation," *IEEE Trans. Magn.*, vol. 38, no. 5, pp. 3177–3179, Sep. 2002.

[21] Z. Shen et al., "The faraday shields loss of transformers," *IEEE Trans Power Electron.*, vol. 35, no. 11, pp. 12194–12206, Nov. 2020.

[22] M. Czerwienku, A. Uramek, and R. P. Wojda, "Derivation of the planar square coil litz-wire winding resistance for sinusoidal currents," *Przeglad Elektrotechniczny*, vol. 95, no. 6, pp. 105–109, 2019.

[23] A. W. Lotfi and F. C. Lee, "A high frequency model for Litz wire for switch-mode magnetics," in *Proc. IEEE Conf. Rec. 1993 Ind. Appl. Conf. 28th IAS Annu. Meeting*, 1993, pp. 1169–1175.

[24] R. P. Wojda and M. K. Kazimierczuk, "Winding resistance of litz-wire and multi-strand inductor," *IET Power Electron.*, vol. 5, no. 2, pp. 257–268, Sep. 2012.

[25] X. Nan and C. R. Sullivan, "An equivalent complex permeability model for litz-wire windings," *IEEE Trans. Ind. Appl.*, vol. 45, no. 2, pp. 854–860, Mar./Apr. 2009.

[26] W. Chen and X. W. Xu, "Solution of Litz wire winding loss based on segmented equivalent circuit method," *Elect. Eng.*, vol. 3, pp. 30–35, 2017.
[27] C. R. Sullivan, "Computationally efficient winding loss calculation with multiple windings, arbitrary waveforms, and two-dimensional or three-dimensional field geometry," *IEEE Trans Power Electron.*, vol. 16, no. 1, pp. 142–150, Jan. 2001.
[28] J. H. Spreen, "Electrical terminal representation of conductor loss in transformers," *IEEE Trans. Power Electron.*, vol. 5, no. 4, pp. 424–429, Oct. 1990.
[29] J. P. Vandelac and P. Ziogas, "A novel approach for minimizing high-frequency transformer copper losses," *IEEE Trans. Power Electron.*, vol. 3, no. 3, pp. 266–277, Jul. 1988.
[30] M. K. Kazimierczuk, *High-Frequency Magnetic Components*. Ogden, Utah: Wiley, 2014, pp. 339–340.
[31] T. Guillod, J. Huber, F. Krismer, and J. W. Kolar, "Litz wire losses: Effects of twisting imperfections," in *Proc. IEEE Workshop Control Model. Power Electron.*, 2017, pp. 1–8.
[32] C. R. Sullivan and R. Y. Zhang, "Simplified design method for litz wire," in *Proc. IEEE Appl. Power Electron. Conf. Expo.*, 2014, pp. 2667–2674.
[33] J. A. Ferreira, "Analytical computation of AC resistance of round and rectangular Litz wire windings," *IEE Proc. B Elect. Power Appl. U.K.*, vol. 139, no. 1, 1992, Art. no. 21.
[34] F. Tourkhani and P. Viarouge, "Accurate analytical model of winding losses in round litz wire windings," *IEEE Trans. Magn.*, vol. 37, no. 1, pp. 538–543, Jan. 2001.
[35] R. P. Wojda and M. K. Kazimierczuk, "Winding resistance and power loss of inductors with litz and solid-round wires," *IEEE Trans. Ind. Appl.*, vol. 54, no. 4, pp. 3548–3557, Jul./Aug. 2018.

Yueyin Wang (Student Member, IEEE) was born in Liaoning, China, in 1996. He received the B.S. degree in electrical engineering and automation from the Shenyang Institute of Engineering, Liaoning, China, in 2018, and the M.S. degree in electrical engineering from the North China Electric Power University, Beijing, China, in 2021. He is currently working toward the Ph.D. degree in electrical engineering with the Southeast University, Nanjing, China.

His research interests include active gate driver technology, converter electromagnetic modeling, and high-frequency transformer.

Wu Chen (Senior Member, IEEE) was born in Jiangsu, China, in 1981. He received the B.S., M.S., and Ph.D. degrees in electrical engineering from the Nanjing University of Aeronautics and Astronautics, Nanjing, China, in 2003, 2006, and 2009, respectively.

From 2009 to 2010, he was a Senior Research Assistant with the Department of Electronic Engineering, City University of Hong Kong, Hong Kong. In 2010–2011, he was a Postdoctoral Researcher with the Future Electric Energy Delivery and Management Systems Center, North Carolina State University, Raleigh, NC, USA. Since September 2011, he has been an Associate Research Fellow with the School of Electrical Engineering, Southeast University, Nanjing, China, where he has been a Professor since 2016. His research interests include soft-switching converters, power delivery, and power electronic system integration.

Dr. Chen serves as an Associate Editor for the IEEE TRANSACTIONS ON INDUSTRIAL ELECTRONICS, *Journal of Power Electronics*, and *CPSS Transactions on Power Electronics and Applications*.

Zhan Shen (Member, IEEE) received the B.E. degree in electrical engineering and automation from the Nanjing University of Aeronautics and Astronautics, Nanjing, China, in 2013, the M.E. degree in electrical engineering from the Southeast University, Nanjing, China, in 2016, and the Ph.D. degree in energy technology from the Aalborg University, Aalborg, Denmark, in 2020.

He is currently an Associate Professor with the Southeast University, Nanjing, China. He was a Visiting Scholar with the RWTH Aachen University, Aachen, Germany, and with the Massachusetts Institute of Technology, Cambridge, MA, USA. He was with the ABB Corporate Research Center, Beijing, China, in 2016. His research interests include power electronic system integration, magnetic components, and artificial intelligence.

Dr. Shen was the recipient of multiple Best Paper and Best Presenter Awards of the IEEE PELS sponsored conferences, and the Outstanding Reviewer Award of the IEEE TRANSACTIONS ON POWER ELECTRONICS.